Remote Sensing of Environment 114 (2010) 2248–2258

Contents lists available at ScienceDirect

Remote Sensing of Environment

journal homepage: www.elsevier.com/locate/rse

Deriving maximal light use efficiency from coordinated flux measurements and satellite data for regional gross primary production modeling

Hesong Wang [a,b], Gensuo Jia [a,*], Congbin Fu [a], Jinming Feng [a], Tianbao Zhao [a], Zhuguo Ma [a]

[a] RCE-TEA, Institute of Atmospheric Physics, Chinese Academy of Sciences, Beijing 100029, China
[b] Graduate University of Chinese Academy of Sciences, Beijing 100049, China

ARTICLE INFO

Article history:
Received 8 January 2010
Received in revised form 30 April 2010
Accepted 2 May 2010

Keywords:
Maximal light use efficiency (ε_{max})
Satellite
Flux site
Gross primary production (GPP)
Modeling
Northern China

ABSTRACT

Remote sensing models based on light use efficiency (LUE) provide promising tools for monitoring spatial and temporal variation of gross primary production (GPP) at regional scale. In most of current LUE-based models, maximal LUE (ε_{max}) heavily relies on land cover types and is considered as a constant, rather than a variable for a certain vegetation type or even entire eco-region. However, species composition and plant functional types are often highly heterogeneous in a given land cover class; therefore, spatial heterogeneity of ε_{max} must be fully considered in GPP modeling, so that a single cover type does not equate to a single ε_{max} value. A spatial dataset of ε_{max} accurately represents the spatial heterogeneity of maximal light use would be of significant beneficial to regional GPP models. Here, we developed a spatial dataset of ε_{max} by integrating eddy covariance flux measurements from 14 field sites in a network of coordinated observation across northern China and satellite derived indices such as enhanced vegetation index (EVI) and visible albedo to simulate regional distribution of GPP. This dynamic modeling method recognizes the spatial heterogeneity of ε_{max} and reduces the uncertainties in mixed pixels. Further, we simulated GPP with the spatial dataset of ε_{max} generated above. Both ε_{max} and growing season GPP show complex patterns over northern China that reflect influences of humidity, green vegetation fractions, and land use intensity. "Green spots" such as oasis meadow and alpine forests in dryland and "brown spots" such as build-up and heavily degraded vegetation in the east are clearly captured by the simulation. The correlation between simulated GPP and EC measured GPP indicate that the simulated GPP from this new approach is well matched with flux-measured GPP. Those results have demonstrated the importance of considering ε_{max} as both a spatially and temporally variable values in GPP modeling.

© 2010 Elsevier Inc. All rights reserved.

1. Introduction

Gross primary production (GPP), the flux of carbon into ecosystems via photosynthetic assimilation, is an important variable in global carbon cycle and a key process in land surface–atmosphere interactions (Coops et al., 2009; Jung et al., 2008). Continuous monitoring of spatial and temporal variations of GPP at regional scale with high accuracy can provide reliable data for carbon-related climate change studies and useful information for ecosystem management. Eddy covariance (EC) flux measurement is one of the best micrometeorological methods for estimating CO_2, water, and energy exchange between the atmosphere and terrestrial ecosystems (Li et al., 2007). It can provide valuable information on daytime GPP by measuring net ecosystem exchange (NEE) and estimating daytime ecosystem respiration at site level (Falge et al., 2002; Falge et al., 2002). Unfortunately, regional extrapolation of field based GPP measurements is still a challenging task due to the high spatial and temporal variability of terrestrial ecosystems across complex landscapes and regions (Maselli et al., 2009).

The application of satellite remote sensing has greatly enhanced global scale observations of vegetation dynamics, and has played an increasingly important role in estimation of GPP and net primary production (NPP) over heterogeneous landscapes. Remote sensing models based on light use efficiency (LUE) integrate satellite observations and ground measurements provide promising tools for regional GPP monitoring (Chasmer et al., 2009; Garbulsky et al., 2008; Landsberg & Waring, 1997; Potter et al., 1993; Prince & Goward, 1995; Running et al., 2004; Veroustraete et al., 2002; Xiao et al., 2004; Xiao et al., 2004). However, in many current LUE-based models, maximal LUE (ε_{max}) heavily relies on vegetation types and is considered as a constant, rather than a variable for a certain vegetation type or even entire eco-region. One obstacle of simulating regional GPP with LUE-based models is the uncertainties in distinguishing real world vegetation types. For most moderate to coarse resolution satellite data (such as MODerate resolution Imaging Spectroradiometer (MODIS)), there exist many mixed pixels with spatial resolutions

* Corresponding author. RCE-TEA, Institute of Atmospheric Physics, Chinese Academy of Sciences, PO Box 9804, Beijing 100029, China. Tel.: +86 10 82995314.
E-mail address: jiong@tea.ac.cn (G. Jia).

0034-4257/$ – see front matter © 2010 Elsevier Inc. All rights reserved.
doi:10.1016/j.rse.2010.05.001

ranging from 250 m to 1000 m. This may contain errors in the assignment of land cover type to a mixed pixel. Moreover, ε_{max} is a changing variable, and its spatial variation and temporal changes are largely influenced by land use change, disturbance history, and different successional stages of vegetation (Yan et al., 2009). So, it is illogical either to employ a fixed ε_{max} to represent certain biome or to reconcile one pixel as one fixed biome pattern. Detailed analyses of the spatial heterogeneity of ε_{max} at regional scale are badly needed for GPP modeling.

Deriving ε_{max} from remotely sensed data could greatly improve the ability of LUE-based model in estimating GPP in regions with heterogonous land cover. A large number of studies have demonstrated positive relationships between vegetation indices (VIs) and LUE (Cheng et al., 2009; Drolet et al., 2005, 2008; Jenkins et al., 2007; Nakaji et al., 2007). In this study, EVI (enhanced vegetation index) was chosen from VIs to simulate LUE considering its great sensitivity to both low and high biomass regions while minimizing soil and atmosphere influences on vegetation monitoring (Huete et al., 2002). Meanwhile, albedo is considered as the primary factor determining the fraction of photosynthetically active radiation (PAR) absorbed (Tian et al., 2004). Albedo modifies the amount of PAR and thus strongly affects vegetation productivity in a given region (Sellers et al., 1997). Here, we chose visible albedo (and combined with EVI) to calculate LUE considering its relevance to photosynthetic active radiation ranging from 400 nm to 800 nm. Consequently, we integrated remote sensing products including maximal EVI and minimal visible albedo of growing season with EC flux measurements to simulate maximal LUE (ε_{max}) for GPP modeling.

In this paper, we simulated GPP in northern China with a gridded parameter of ε_{max} retrieved from remote sensing data with full consideration of its heterogeneous nature. We firstly used a dynamic modeling method that combines maximal EVI and minimal visible albedo of growing season to retrieve ε_{max} for each pixel in the region. Compared to the treatment of ε_{max} in most current LUE-based models, this method considers ε_{max} as a variable at pixel scale and doesn't solely rely on land cover types. The ε_{max} we retrieved was also compared with those used for MODIS GPP algorithm (MOD17). Then, we simulated GPP in growing season of 2008 and validated the results with GPP retrieved from flux measurements. Finally, we analyzed the spatial patterns of ε_{max} and sum of GPP in growing season over the study area. The results of this study will likely improve carbon cycle modeling by capturing finer patterns with an integrated method of remote sensing and eddy flux measurements.

2. The study site and data

2.1. Site description

Field measured GPP, air temperature, solar radiation, and PAR were collected from the 14 field EC flux sites under a coordinated enhanced observation project in arid and semi-arid regions in northern China (Table 1). These 14 flux sites represent the dominant vegetation/land cover types in the region: temperate grassland, cropland, deciduous broadleaf forests, and evergreen needleleaf forests. For croplands, all the 5 sites (including Jinzhou (JZ), Linze (LZ), Tongyu-Crop (TYC), Dingxi (DX) and Yingke (YK)) are irrigated with intensive management. JZ, LZ and YK are planted with maize (*Zea mays*), TYC is planted with sunflower (*Helianthus annuus*) and DX is planted with wheat (*Triticum aestivum*). For forests, Dayekou (DYK) is a sub-alpine evergreen needleleaf forest site, while Changwu (CW) and Miyun (MY) are deciduous broadleaf forest sites. For grasslands, Arou (AR) is a sub-alpine meadow site, Zhangye (ZY) represents steppe desert, Tongyu-Grass (TYG) represents degraded meadow steppe, Yuzhong (YZ) represents typical steppe, Dongsu (DS) represent desert steppe, while Naiman (NM) is a sandy grassland site.

Table 1
Main characteristics of the 14 flux sites in the study region.

Site	Vegetation type	Location	EC above canopy (m)	Elevation (m)	Precipitation (mm)
JZ	Cropland (maize)	41°09 N, 121°12E	1	17	463
YK	Cropland (maize)	38°51 N, 100°15E	1	2859	382
LZ	Cropland (maize)	39°20 N, 100°25E	1	1382	376
TYC	Cropland (sunflower)	44°35 N, 122°52E	2	151	404
DX	Cropland (wheat)	35°33 N, 104°36E	2	1912	505
ZY	Steppe desert	39°05 N, 100°16E	2	1483	353
DS	Desert steppe	44°05 N, 113°34E	2	990	287
TYG	Degraded meadow steppe	44°34 N, 122°55E	2	151	404
AR	Sub-alpine meadow steppe	38°03 N, 100°28E	2	3033	396
YZ	Typical steppe	35°57 N, 104°08E	2	1968	382
NM	Desert steppe	42°56 N, 120°42E	2	371	405
DYK	Evergreen needleleaf forest	38°32 N, 100°15E	10	2823	360
CW	Deciduous broadleaf forest	35°15 N, 107°41E	20	1220	540
MY	Deciduous broadleaf forest	40°38 N, 117°19E	25	350	584

2.2. Field measurements and data quality control

The EC systems, which were mounted above canopy from 1 to 25 m (Table 1), consist of a three-dimensional sonic anemometer (Model CSAT3, Campbell Scientific Inc., Logan, Utah, USA except for LZ and CW which adopt WindMaster from Gill Instruments Ltd. Lymington, Hampshire, UK) and an open-path fast response infrared gas analyzer (IRGA, Model LI7500, LI-Cor Inc., Lincoln, Nebraska, USA). The raw data were recorded at a rate of 10 Hz, and the computations were done for each 30 min period by a Data-Logger (Model CR5000, Campbell Scientific Inc., Logan, Utah, USA). Intensive calibration was done weeks before the coordinated enhanced observation period (July to September, 2008) to ensure proper performance of the instruments and to make those site scale data comparable.

Webb, Pearman and Leuning (WPL) term (Webb et al., 1980) that accounts for errors introduced by fluctuations in water vapor density and temperature was applied to correct net ecosystem exchange (NEE) time series directly measured by EC. The periods of half-hour bad data caused by water vapor condensation and raindrops on the windows of the open-path infrared gas analyzer were removed. To fill small blocks (less than a few hours) of missing and bad data, a linear interpolation method was applied to each time series. Larger gaps were filled with values derived from the Michaelis–Menten equation of PAR (Falge et al., 2001). More details on data quality control have been described by Liu et al. (2008). NEE measured by EC in nighttime is treated as ecosystem respiration since photosynthesis is almost zero. The daytime respiration is calculated with the Q_{10} of respiration in nighttime when EC measures gross respiration without considering photosynthesis (Falge, Baldocchi, et al., 2002; Falge, Tenhunen, et al., 2002). GPP was finally estimated as NEE minus estimated daytime ecosystem respiration ($R_{Day\text{-}eco}$):

$$GPP = -\left(NEE - R_{Day-eco}\right). \quad (1)$$

Then, daily GPP were accumulated to 8-day integrated GPP to be consistent with MODIS 8-day products.

2.3. Ancillary meteorology data

The raster datasets of daily air temperature and PAR were interpolated spatially using kriging from the air temperature and solar radiation measured at 390 meteorological stations in northern China at the same resolution of surface reflection (MOD09A1, 500 m). Solar radiation is assumed as a linear function of PAR, and a conversion of 2.05 was taken from 10^6 Joules (10^6 J) to mol PAR (Aber et al., 1996). The air temperature and solar radiation data over the region were provided by China meteorological data service (http://data.cma.gov.cn). Daily air temperature and PAR were also averaged to 8-day intervals to be consistent with MODIS 8-day composites.

2.4. Remotely sensed data

The digital elevation model (DEM) data was obtained from U.S. Geological Survey (USGS) global DEM dataset (http://rmmcweb.cr.usgs.gov/elevation/) for analyzing terrain features of the study area. The MODIS Land products (Collection 5) were provided by MODIS Land Team (http://modis-land.gsfc.nasa.gov/) and include surface reflection (MOD09A1) and Land cover types (MCD12Q1). MOD09A1 was selected to generate spatial dataset of visible albedo (Liang, 2000), land surface water index (LSWI), and enhanced vegetation index (EVI) in northern China with a temporal resolution of 8 day and spatial resolution of 500 m, over the coordinated enhanced observation period (July to September, 2008). 2008 land cover data (MCD12Q1) was selected to analyze the feature of $\varepsilon_{\max}$ for different land cover categories:

$$albedo_{\text{visible}} = 0.331\rho_1 + 0.42\rho_3 + 0.246\rho_4 \tag{2}$$

$$LSWI = \frac{\rho_2 - \rho_6}{\rho_2 + \rho_6} \tag{3}$$

$$EVI = \frac{G \times (\rho_2 - \rho_1)}{(\rho_2 + (C_1 \times \rho_1 - C_2 \times \rho_3) + L)} \tag{4}$$

Table 2
Parameters of the Landsat images for evaluating landscape heterogeneity around the flux towers.

Site	Sensor	Path/row	Acquisition time
AR	Landsat-5 TM	133/34	2009-8-11
DYK	Landsat-5 TM	133/33	2009-8-11
JZ	Landsat-5 TM	120/31	2009-7-15

where, visible albedo ($albedo_{\text{visible}}$) was derived from three visible bands from MOD09A1. $\rho_1, \rho_2, \rho_3, \rho_4$ and ρ_6 are the reflectance bands in MOD09A1: blue band (459–478 nm), green band (545–565 nm), red band (620–670 nm), near infrared band (841–875 nm), and short-wave infrared band (1628–1652 nm) respectively. LSWI is sensitive to changes in leaf water content over time (Maki et al., 2004; Xiao, Hollinger, et al., 2004). The coefficients adopted in the EVI algorithm are: $L = 1$, $C_1 = 6$, $C_2 = 7.5$ and G (gain factor) $= 2.5$ (Huete et al., 2002). EVI includes the blue band for atmospheric correction, which has been used for the study of vegetation dynamics or production recently (Sims et al., 2006; Zhang et al., 2003, 2008).

We selected 3×3 subsets (approximately 1.5×1.5 km^2) of MOD09A1 in the period of coordinated flux measurements that centered on the eddy flux tower sites of this study from Oak Ridge National Laboratory (ORNL). Two major factors, footprint of flux and geo-location accuracy of satellite products, were considered when we decided the size of subsets. Details on footprint analysis will be provided in the following sections. We generated spatial datasets of EVI and visible albedo from product MOD09A1 to connect the flux-measured $\varepsilon_{\max}$ with remote sensing data (for more details, see the next section).

Additionally, three cloud free scenes of Landsat Thematic Mapper (TM5) data over the flux stations AR, DYK and JZ in summer of 2009 were acquired to evaluate the influence of landscape heterogeneity around the flux towers on the predictability of GPP (Table 2).

3. Methods

3.1. ε_{max} modeling

In this study, the $\varepsilon_{\max}$ of the 14 flux sites were calculated from Michaelis–Menten light response function:

$$NEE = -\left(\frac{\varepsilon_{\max} \times PAR \times GEE_{\max}}{\varepsilon_{\max} \times PAR + GEE_{\max} - R}\right) \tag{5}$$

where, $\varepsilon_{\max}$ is maximal light use efficiency for a certain type of vegetation at canopy scale, PAR is photosynthetic active radiation, $GEE_{\max}$ is the ecosystem gross primary productivity at "saturating" light, and R is ecosystem respiration. $GEE_{\max}$ and $\varepsilon_{\max}$ were all obtained from the GPP measured from flux stations and the fit curves of PAR based on the nonlinear model of Michaelis–Menten function Eq. (5).

We performed regression analysis between the calculated $\varepsilon_{\max}$ and remote sensing products. The remote sensing products include the maximal EVI (MaxE) and minimal visible albedo (MinVa) in growing season and the subsets were chosen from 3×3 pixels (1.5×1.5 km^2) around each flux tower. The results indicate that $\varepsilon_{\max}$ and MaxE had a strong positive relation, while $\varepsilon_{\max}$ and MinVa had strong negative relation (Fig. 1).

Independent variables employing MaxE alone, MinVa alone, and a combination of the former two variables for GPP estimation were compared to get the optimal input (Table 3). The result shows that the combination of MaxE and MinVa can reasonably better simulate $\varepsilon_{\max}$ than taking either of the variables alone, as indicated by its highest R^2 and lowest RMSE. Furthermore, partial correlation of the multi-regression indicates that MaxE and MinVa have nearly the same contribution in modeling $\varepsilon_{\max}$. Therefore, the $\varepsilon_{\max}$ was calculated with the combination of MaxE and MinVa as:

$$\left\{ \varepsilon_{\max} = \exp(1.428MaxE - 6.295MinVa - 1.211),\ MaxE > 0.07 \varepsilon_{\max} = 0, MaxE \le 0.07 \left(R^2 = 0.86,\ p < 0.01\right) \right. \tag{6}$$

Here we define a value of MaxE as 0.07 from desert area as the threshold of vegetation by analyzing seasonal EVI curves throughout the region. MaxE and MinVa are the maximal EVI and minimal visible albedo of the growing season for each pixel respectively.

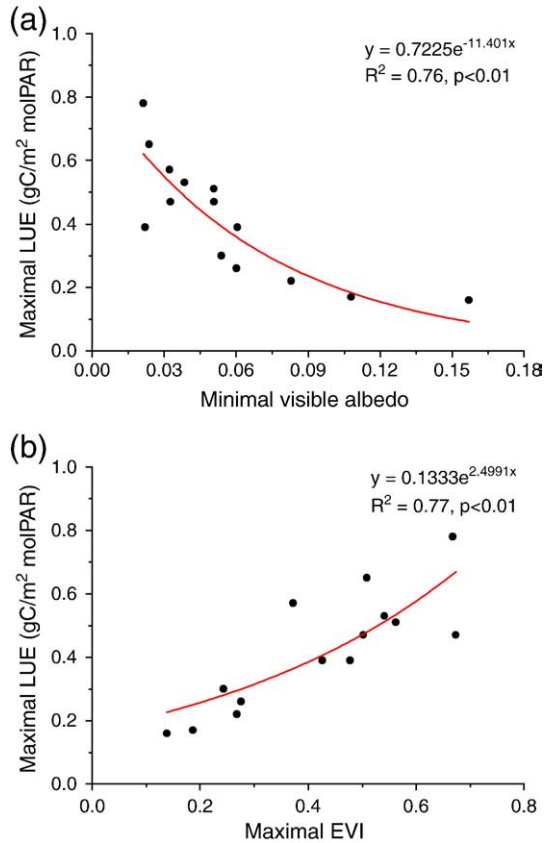

Fig. 1. (a) The negative relationship between maximal light use efficiency (ε_{max}) and minimal visible albedo in growing season; and (b) the positive relationship between ε_{max} and maximal EVI in growing season.

3.2. Description of the VPM model

Vegetation Photosynthesis Model (VPM) is a LUE-based, remote sensing oriented model developed by Xiao et al. (2004)and Xiao et al., (2004). VPM was proposed by the conception of partitioning of vegetation canopies into photosynthetically active vegetation (PAV) such as chloroplasts and non-photosynthetically active vegetation (NPV) such as stem, branch and cell wall:

$$GPP = \varepsilon_g \times FAPAR_{PAV} \times PAR \tag{7}$$

$$\varepsilon_g = \varepsilon_{max} \times T_{scalar} \times W_{scalar} \times P_{scalar} \tag{8}$$

where PAR is photosynthetic active radiation, $FAPAR_{PAV}$ is the fraction of PAR absorbed by leaf chlorophyll of canopy (PAV), and ε_g is actual light use efficiency under environmental stress (Okin, 2007). The parameter ε_{max} is maximal light use efficiency, and T_{scalar}, W_{scalar} and P_{scalar} are the environmental stress indices of temperature, water and leaf phenology on light use efficiency respectively (see Xiao et al., 2004; Xiao et al., 2004 for more details).

3.3. Regional GPP modeling

Regional GPP was simulated by VPM algorithm with modified raster layer of ε_{max} that we generated above except for T_{scalar} algorithm (Fig. 2). The reason for such treatment is that at large regional scale, it is unpractical to get the "three base point" (minimal, maximal and optimal temperature for photosynthesis) to calculate T_{scalar}. So we introduced the algorithm of T_{scalar} in Carnegie–Ames–Stanford Approach (CASA) to

Table 3
Correlations and root mean square errors (RMSEs) of different parameters employed to estimate maximal light use efficiency (gC/Mol PAR): (1) maximal EVI in growing season (MaxE); (2) minimal visible albedo in growing season (MinVa); and (3) combination of MaxE and MinVa.

MaxE		MinVa		MaxE and MinVa			
						Partial correlation	
R^2	RMSE	R^2	RMSE	R^2	RMSE	MaxE	MinVa
0.762	0.136	0.769	0.162	0.86	0.098	−0.628	0.643

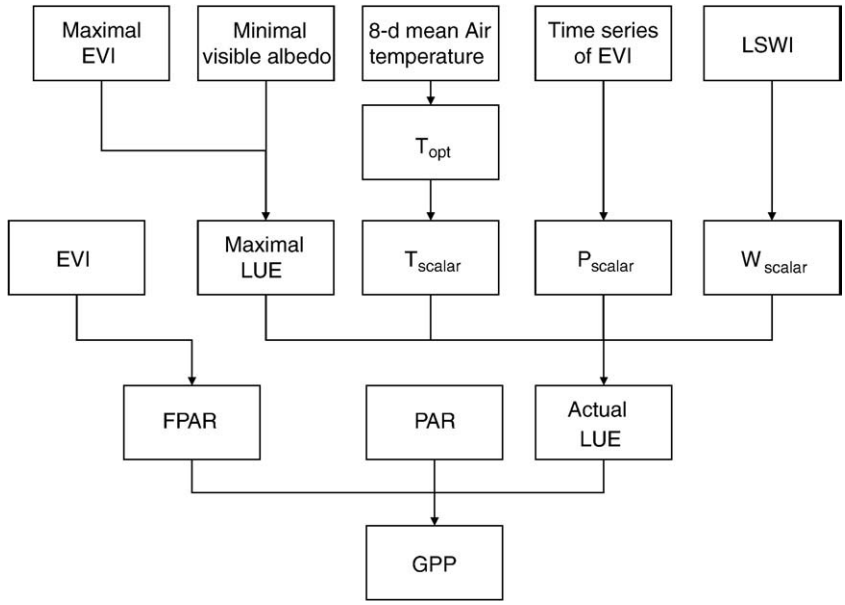

Fig. 2. Flowchart of gross primary production (GPP) modeling method. ε_{max} was retrieved from maximal EVI and minimal visible albedo in growing season; T_{scalar} was calculated from 8-day mean air temperature, T_{opt} was defined as the air temperature when the pixel's EVI reach the peak of the year; P_{scalar} was calculated from the time series of EVI, the period of pixel's EVI exceed the average value of EVI was defined as the expansion period; W_{scalar} was calculated from LSWI; and FPAR was set as the value of EVI.

replace VPM in the case. The alternative algorithm only needs input of optimal temperature for vegetation growth, which is defined as the 8-day air temperature when EVI reaches maximum of the year for each pixel:

$$T_{scalar} = \frac{1.2 \times \left(0.8 + 0.02T_{opt} - 0.0005T_{opt}^2\right) \times \left(1 + \exp\left(0.3 \times \left(T - T_{opt} - 10\right)\right)\right)}{1 + \exp(0.2 \times (T - 10 - T))} \tag{9}$$

where, T_{opt} is the optimal temperature and T is 8-day mean air temperature. If T is lower than 0 °C, T_{scalar} is set as 0; if T_{scalar} is greater than 1, T_{scalar} is set as 1 (Potter et al., 1993).

For each pixel, we defined the period from the turning date when EVI exceeds the average value over growing season to the turning date when EVI drops to this threshold as the state of leaf full expansion. P_{scalar} was set as 1 during this period; for other periods, P_{scalar} was set as $(1 + \mathrm{LSWI})/2$.

3.4. Footprint modeling

A footprint size and shape depend on the diffusion height of the EC measurement, canopy roughness, and planetary boundary layer mixing conditions. In this study, we analyzed the flux footprints with Eulerian analytical approach. The approach assumes stand power law

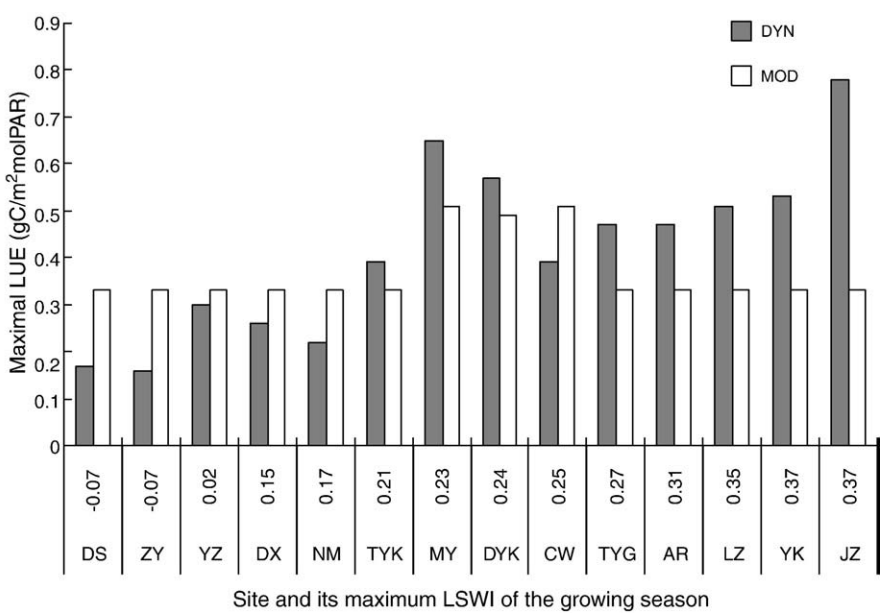

Fig. 3. The maximal light use efficiencies retrieved from flux measurements (ε_{max}-EC) and look-up-tables of MOD17 (ε_{max}-MOD) among different biomes and flux sites along the gradient of humidity.

to obtain vertical profile of the horizontal wind velocity and the eddy diffusivity. Linkage of power law profiles to Monin–Obukhov similarity profiles leads to an analytical solution of the flux footprint, the upwind distance, and the diffusion height. We calculated the size and extent of flux footprint for each of the EC tower and overlaid vector layers on fine resolution satellite images to demonstrate source of EC signals.

4. Results

4.1. Variations of ε_{max} in different biomes

The values of ε_{max} derived from coordinated EC flux measurements (ε_{max}-EC) and MOD17 algorithm (ε_{max}-MOD) were ordered along environmental gradients of humidity and the maximum LSWI in growing season (Fig. 3). ε_{max}-EC showed an increasing trend along the gradient of humidity. However, ε_{max}-MOD was not so sensitive to humidity as ε_{max}-EC. They barely agree with each other not only between different biomes but also within a certain biome. In croplands, ε_{max}-EC differed largely from 0.26 to 0.78 gC/mol PAR for different crop species planted. Even in the croplands planed with the same crop (JZ, LZ and YK), ε_{max}-EC ranged largely from 0.51 to 0.78 gC/mol PAR. In most cases, ε_{max}-EC was greater than MOD17 derived ε_{max} (ε_{max}-MOD) over cropland sites. For grasslands, although mean value of ε_{max}-EC was similar to ε_{max}-MOD, there still exists a large variation of ε_{max}-EC ranging from 0.16 to 0.47 gC/mol PAR. There was a major difference in ε_{max}-EC between two DBF sites (CW and MY) too. These large variations of ε_{max} between and within biomes indicated that ε_{max} is a variable rather than a constant for a certain biome or even a certain vegetation type. Employing a constant ε_{max} for a certain biome may bring errors for LUE-oriented GPP modeling, although the calculation of absorbed fraction of PAR partly compensated the errors by considering the heterogeneous character of land cover types.

4.2. Spatial patterns of ε_{max}

The raster layer of ε_{max} for northern China in 2008 was derived with the modeling algorithm as described above. Meanwhile, another spatial dataset of ε_{max} was generated from look-up-tables (LUT) according to MODIS derived land cover types (MCD12Q1) in the same period with MOD17 algorithm, which assigned ε_{max} of each pixel according to land cover types (Fig. 4). Both of the ε_{max} spatial datasets captured the key spatial patterns of ε_{max} in the region: ε_{max} is generally greater in the eastern part of the region than in the west. However, the spatial patterns of ε_{max} modeled by our dynamic method (ε_{max}-Dyn) and ε_{max}-MOD were different in the following aspects: 1) ε_{max}-Dyn presented much clearer spatial continuity, i.e., the values of ε_{max}-Dyn gradually decreased from east to west in general, following the gradients of humidity, vegetation cover, and land use options. ε_{max}-Dyn can well capture the mixed ε_{max} over mosaics of different land cover/vegetation classes. By contrast, ε_{max}-MOD had a uniform value in a given biome. The spatial pattern of ε_{max}-MOD exhibited discrete characteristics between different

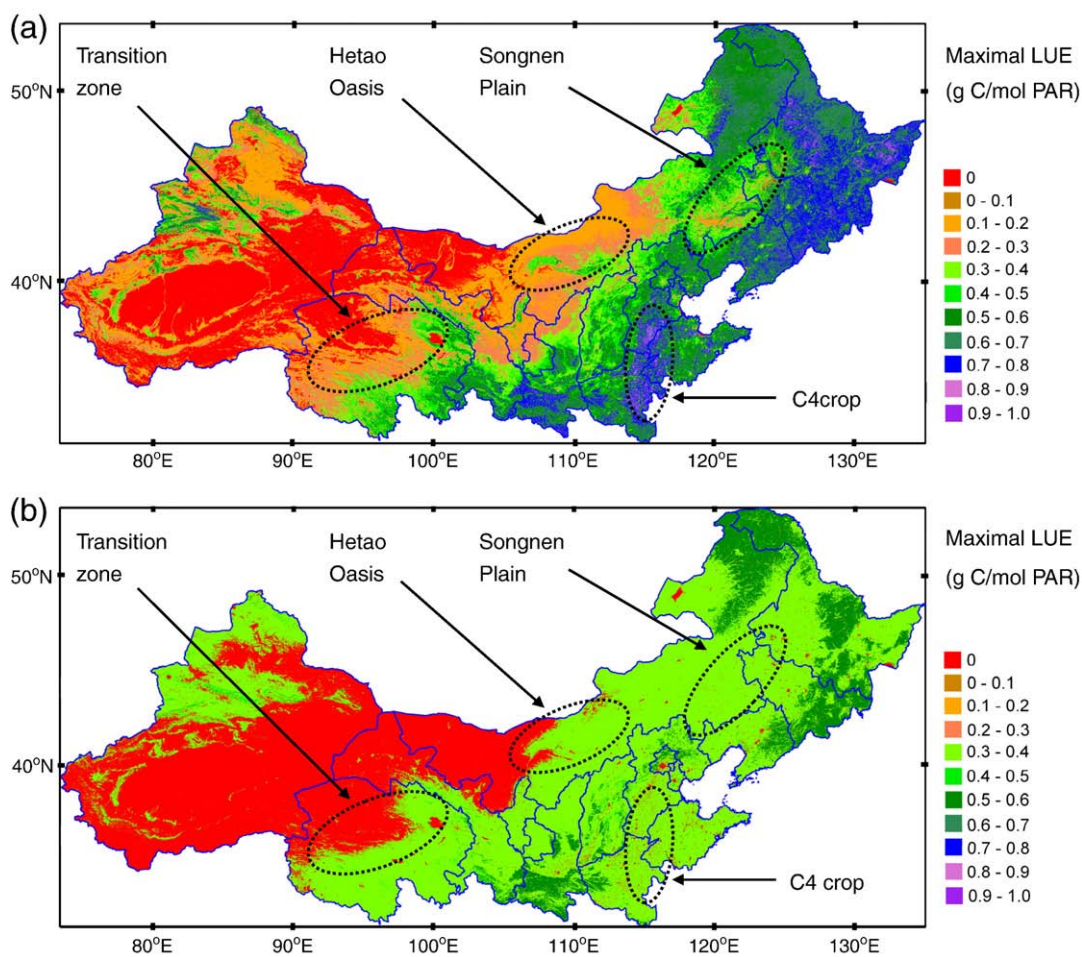

Fig. 4. Spatial patterns of ε_{max} in 2008: (a) retrieved from the simple dynamic modeling method; and (b) retrieved from the MOD17 algorithm with land cover types in 2008.

biomes. There was no transition between vegetated area (mainly grassland or cropland) and barren or sparsely vegetated (BSV) areas since the ε_{max} were all assigned as 0.33 gC/mol PAR in grasslands and croplands, while BSV was assigned as zero. 2) In many areas of BSV, especially those in transitional areas between grassland and desert, vegetation productivity can hardly be ignored, therefore, assigning a fixed ε_{max} (zero) will likely lead to underestimation of GPP over large areas. Another example is land cover class of urban and build-up (UBU). In this case, urban greens and city parks that are commonly found in most urban areas are totally ignored by traditional LUE-GPP modeling efforts when those pixels are categorized as UBU and therefore were assigned as zero in ε_{max}-MOD because land cover types of BSV or UBU were treated as no vegetation activity. 3) The spatial dataset of ε_{max}-Dyn can capture fractional green vegetation in isolated patches over contrasted background, such as oasis in desert and sub-alpine forest/meadow (i.e., Hetao Oasis in Fig. 4) in dryland areas. Those patches often repeatedly cover small areas (sub-pixel in many cases) and are very easy to be ignored in the ε_{max}-MOD approach. 4) Different plant functional types (PFT) in the same biome such as C4 plants in croplands and sandy shrubs in grasslands could also be captured by ε_{max}-Dyn. C4 crops are widely planted in the southeast part of northern China, with higher ε_{max} than most C3 crops. ε_{max}-Dyn can well distinguish C3 and C4 plant in cropland in values of ε_{max}, while ε_{max}-MOD treats ε_{max} for all cropland as the same value. Also, ε_{max}-Dyn sensed the low productivity areas of sandy desert or salty patches in grasslands, which are often ignored by ε_{max}-MOD methods.

Table 4 listed the average value of ε_{max}-Dyn and ε_{max}-MOD for major land cover types of the study area. In general, ε_{max}-Dyn was greater than ε_{max}-MOD, especially for cropland, deciduous broadleaf forest (DBF), and mixed forest (MF), while evergreen needleleaf forest (ENF), deciduous needleleaf forest (DNF) and grassland had closer values between them.

4.3. Spatial patterns of GPP

With the modified raster layer of ε_{max}-Dyn, we simulated 8-day GPP time series over 2008 growing season and generated a spatial dataset of accumulative GPP in growing season (Fig. 5). The GPP in northern China followed a clear longitudinal gradient and increased from west to east and from lowland to high plateaus, likely controlled by the gradient of humidity, green vegetation fractions and land use intensity. In 2008, the average GPP in growing season was 509.29 gC/m^2 for the entire region. High GPP areas mainly distributed in the eastern part of northern China where forest and cropland dominate, but the "brown spots" such as build-up and heavily degraded vegetation in this area can also be clearly captured by the simulated GPP. In the central part of the region, GPP dropped gradually from east to west, as dense grasslands were gradually replaced by sparse grasses and shrubs towards inland. However, high GPP areas were often found over cultivated areas, sub-alpine forest/meadow, and oasis. In the western part of the region, the dominant land cover type was BSV, with the lowest GPP. Also, some croplands, grasslands and ENF existed in oasis or sub-alpine regions and became "green spot" with high GPP even in vast Gobi desert (Fig. 5). In some cases, GPP values over oasis and major river valleys in western desert were even higher than central grassland.

GPP is largely a function of dominant vegetation types in a given area or pixel. Areas dominated by deciduous broadleaf forests and coniferous forests generally had the highest GPP, while cropland took the second place likely due to its intense management and dense crown cover, followed by lower coverage vegetation (such as urban greens and open shrubland) and grassland. BSV had the lowest GPP but can still be detected by our modeling method (Table 5).

4.4. Accuracy assessment of GPP simulation

We calculated the mean value of simulated GPP over 3×3 pixel subsets (1.5×1.5 km^2) around flux sites to perform liner regression with correspondent field measured GPP to assess accuracy. Sums and the relative errors between EC measured and model simulated GPP for different land cover types indicated that the GPP was simulated with reasonable accuracy (Table 5). The liner regression model also showed a good agreement among different land cover types (Fig. 6). For all sites, the correlation had a good agreement and highly significant level ($R^2=0.78$, $p<0.01$). As to different land cover types, grass sites had the highest correlation with highly significant ($R^2=0.82$, $p<0.01$), crop sites took the second place ($R^2=0.69$, $p<0.01$) and forest sites had the lowest correlation with moderate significant ($R^2=0.60$, $p<0.05$).

5. Discussion and conclusions

The differences in the performance of our GPP modeling among different land cover types or locations were partly contributed by the landscape heterogeneity over flux sites. Heterogeneity within the subset around flux towers would influence the correlation between field measurements and remote sensing simulation due to mismatch in spatial representative areas (Wu et al., 2009). We chose grassland site AR, cropland site JZ and forest site DYK as examples to analyze influence of landscape heterogeneity on the performance of GPP simulation (Fig. 7). DYK had the lowest correlation among the 3 sites, JZ took the second place and AR had the highest correlation. From the EVI histogram of the subsets and landscape views from Landsat high resolution image (TM5), it is very clear that greater landscape heterogeneity often leads to lower agreement between pixel scale GPP simulation and site scale field measurements. Here, DYK is categorized as a sub-alpine ENF site, however, in 1.5×1.5 km^2 subset (equal to the 3×3 pixels of spatial GPP dataset) around the flux site at least three different vegetation types mixed as a mosaic, which are dense needleleaf forest on shady slopes, sparse deciduous shrubs on sunny slopes and sub-alpine meadows on flat tops. The EVI histogram of the subset of high resolution image (TM5) ranged from 0.1 to 0.5, more than half of the pixels have EVI values ranging from 0.1 to 0.3, which were mainly contributed by sparse vegetation. Such a

Table 4
Comparison of GPP in growing season, the maximal light use efficiency retrieved from simple dynamic modeling method (ε_{max}-Dyn) and look-up-tables of MOD17 (ε_{max}-MOD) of the main land cover types over northern China.

Biome type	GPP (gC/m^2)	ε_{max}-DYN (gC/mol PAR)	ε_{max}-MOD (gC/mol PAR)	Areas fraction (%)
ENF	581.42	0.42	0.49	0.51
DNF	937.40	0.58	0.54	1.04
DBF	1680.93	0.71	0.51	2.50
MF	1320.83	0.64	0.54	6.05
Oshrub	254.53	0.27	0.38	2.52
Grass	364.55	0.33	0.33	27.90
Crop	1041.95	0.60	0.33	18.48
UBU	397.96	0.36	0.00	0.79
BSV	30.57	0.06	0.00	32.96

Biome class key: ENF = evergreen needleleaf forest; DNF = deciduous needleleaf forest; DBF = deciduous broadleaf forest; MF = mixed forest; Oshrub = open shrubland; Grass = grassland; Crop = cropland; UBU = urban and built-up; BSV = barren or sparsely vegetated.

Table 5
Sums and the relative errors between EC measured and modeled GPP in different biomes.

	Measured GPP (gC/m^2/8-day)	Simulated GPP (gC/m^2/8-day)	Relative error (%)
Grass sites	20.56	22.83	11.06
Forest sites	36.47	42.96	17.80
Crop sites	65.76	61.06	−7.14
All sites	40.93	42.28	3.31

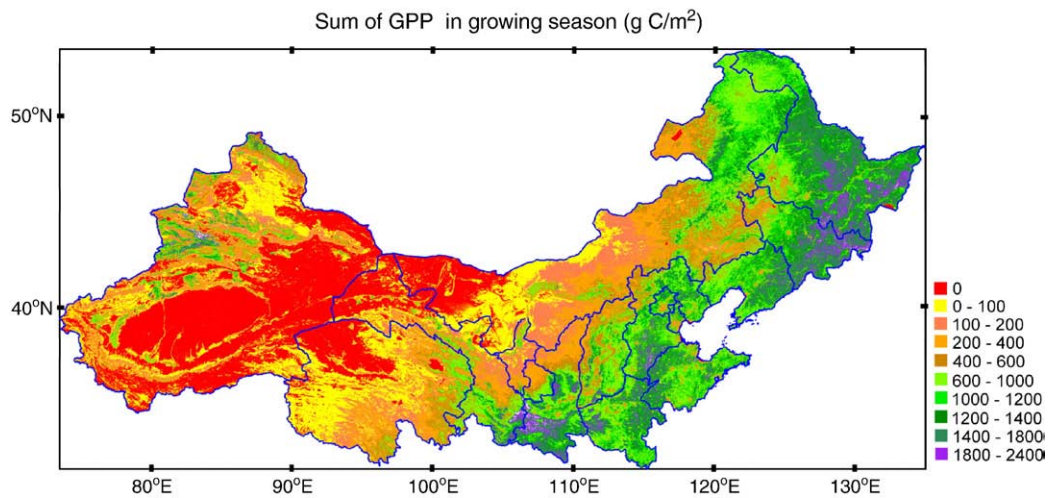

Fig. 5. Spatial patterns of sum of GPP in growing season (from April to September).

heterogeneous pattern will very likely influence the performance of VPM up-scaling of GPP from site scale to regional scale. For JZ, EVI values of correspondent pixels ranged from 0.4 to 0.6, but there were still large fractions of low EVI values contributed by build-up and bare soil around croplands, which influenced the correlation moderately; for AR, the land cover can be considered as relatively homogenous, with nearly all EVI signature contributed by sub-alpine meadow, ranging from 0.3 to 0.5, which will likely lead to more accurate simulation and up-scaling by VPM model. The footprint analysis illustrated the same issue, although the source area of DYK was mainly contributed by forest, but it also mixed with grassland, bare land, and even river; JZ's source area of cropland was also mixed by buildings and roads; as to AR, the source area was entirely contributed by a pure signal of grassland (Fig. 8).

Another source that may influence the performance of GPP modeling was the flux measurement itself. EC measures GPP indirectly by calculating it from flux-measured NEE and estimates daytime ecosystem respiration. However, instrument calibration and data quality control are critical for NEE measurements. Daytime ecosystem respiration was estimated by extrapolating the relationship between nighttime respiration and soil temperature to daytime. Both NEE and respiration require subjective decisions and are currently the subject of a great deal of discussion (Falge, Baldocchi, et al., 2002; Falge, Tenhunen, et al., 2002). Here, we calibrated key EC instruments and performed a

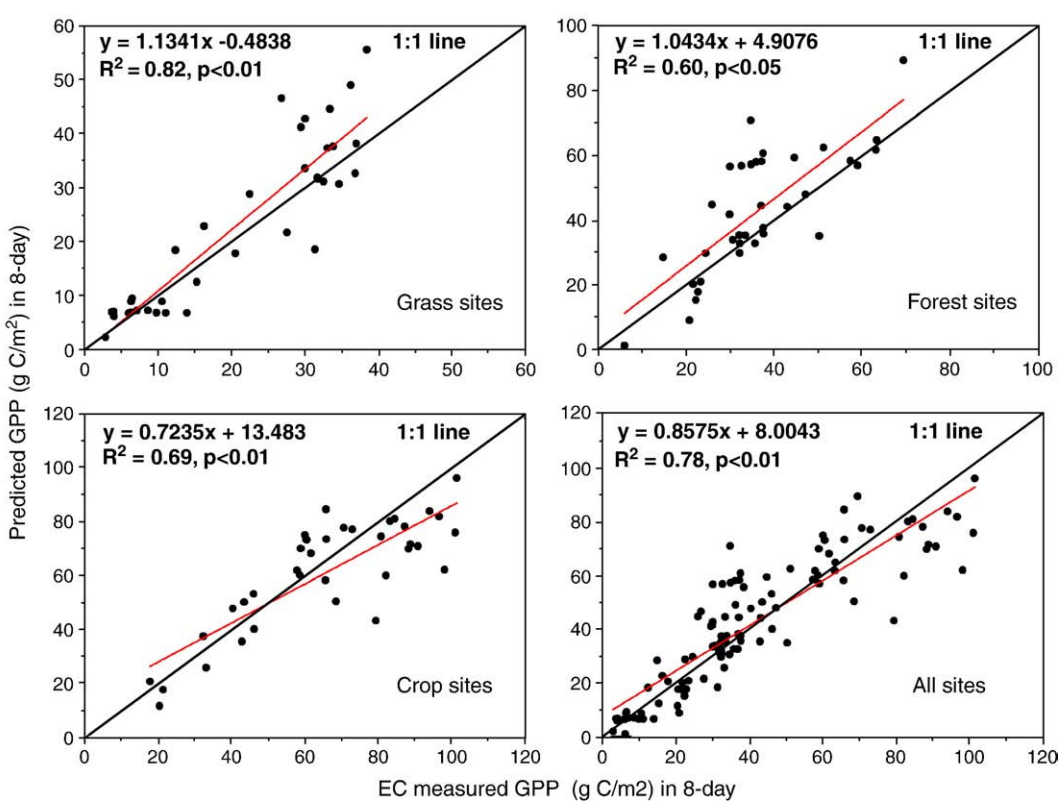

Fig. 6. Comparison between the observed GPP and modeled GPP in northern China.

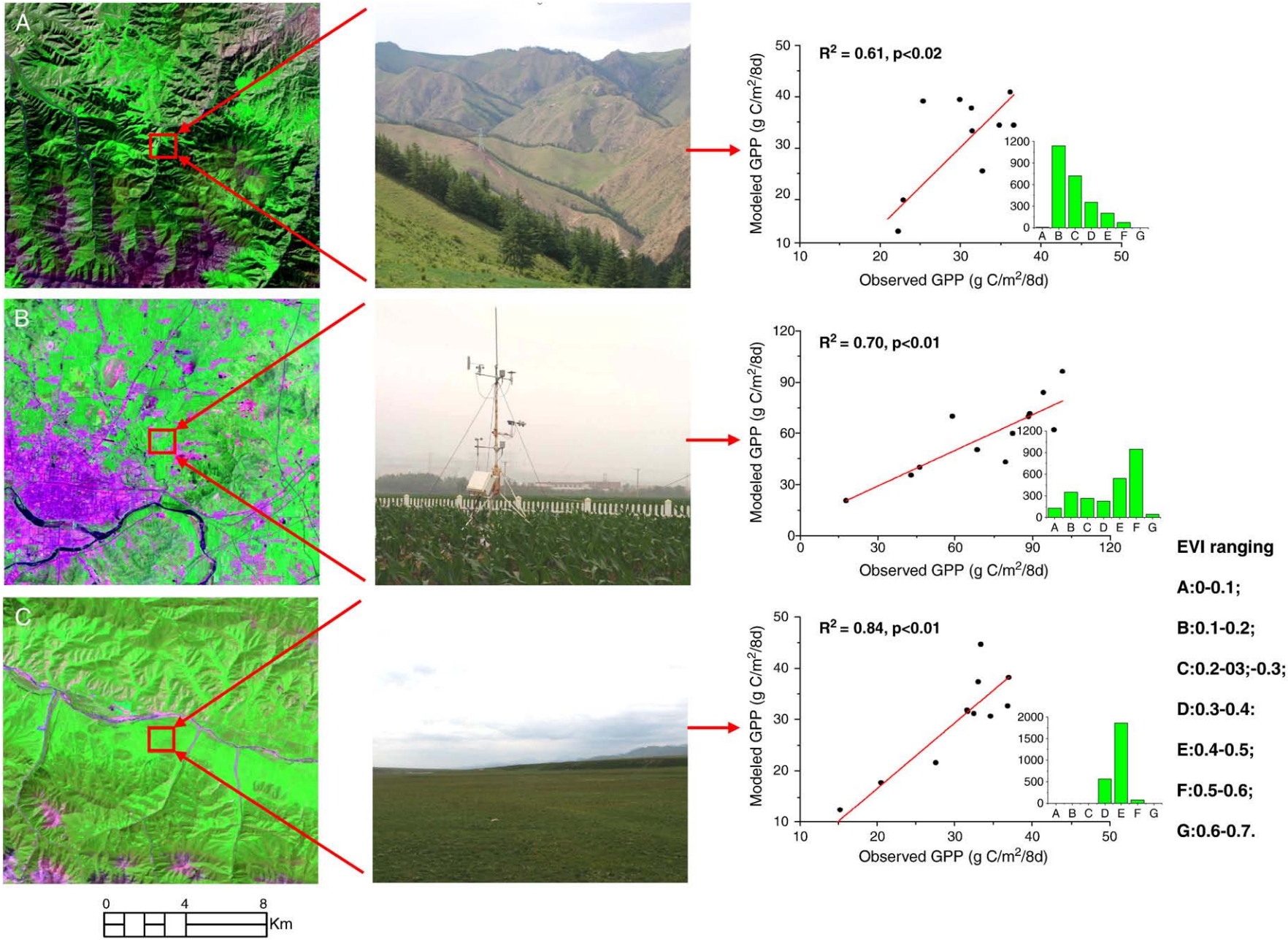

Fig. 7. Landscape views from satellite, site underlying surface pictures, regression relationships between modeled and observed GPP and the histograms of EVI of the subset with the size of 1.5×1.5 km^2 around the site. (A) DYK, (B) JZ and (C) AR. The range of EVI was expressed as alphabet, A: 0–0.1; B: 0.1–0.2; C: 0.2–0.3; D: 0.3–0.4; E: 0.4–0.5; F: 0.5–0.6; G: 0.6–0.7.

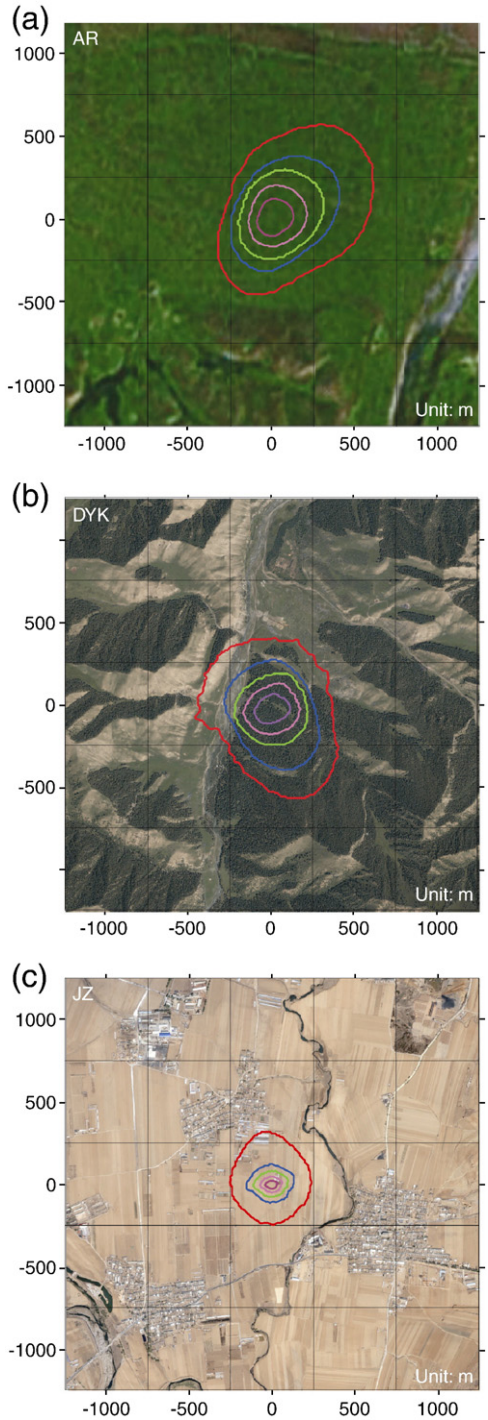

Fig. 8. Footprint of the observation period in (a) DYK, (b) JZ, and (c) AR. The size of the grid is 0.5×0.5 km^2, and the key of the contour line for percentage of total footprint is: purple = 60%, magenta = 80%, green = 90%, blue = 95%, and red = 99%.

coordinated quality control for all participant sites (14 in total) to improve the quality and consistency of our sites during the enhanced coordinated observation period. Meanwhile, intensified post-calibration and data quality control also greatly improved the reliability of our EC measurements and reduced uncertainty related to instruments, field protocol, and missing/bad data.

We also compared our simulation results with both ε_{max}-MOD and previous field EC measurements in the region. Field EC measured ε_{max} of needleleaf forest from previous studies ranged from 0.62 to 0.83 gC/mol PAR (Wu et al., 2009), while the ε_{max} values for croplands in northern China ranged from 0.76 to 0.92 gC/mol PAR with the same method (Yan et al., 2009). ε_{max}-Dyn are much closer to those results than ε_{max}-MOD in the corresponding land cover type, although it is still lower than those field based results. It is likely due to the fact that ε_{max}-Dyn we calculated are still average values in a given pixel (large area), and often mixed with signals of lower vegetation productivity.

The MODIS derived GPP is one of the main sources of satellite-based products for vegetation processes that cover entire globe with 8-day MVC composite at 1 km pixel resolution. However, several recent studies have highlighted limitations of this product and the models used to derive the dataset (Heinsch et al., 2006; Running et al., 2004; Turner et al., 2003, 2005; Yan et al., 2009). The underestimates of vegetation productivity by MODIS GPP products in high productivity areas are very likely contributed by the relatively low value of ε_{max} based on the standard MODIS-based GPP/NPP algorithm (MOD17, Running et al., 1999). Further, MOD17 doesn't distinguish major crop species and plant functional types, which could lead to errors in GPP modeling among different ecological categories. This is likely due to lack of calibration data collected from East Asia used in the MOD17, and that the parameters in MOD17 might be not suitable for our study region. In this study, we integrated a network of flux measurements with remote sensing data to retrieve high accuracy spatial data of regional GPP and hope to cope with those problems.

Site-specific LUE-based models such as VPM has been evaluated successfully by using ε_{max} retrieved from flux tower data for various land cover/vegetation classes (Li et al., 2007; Wu et al., 2009; Xiao et al., 2004; Xiao et al., 2004; Yan et al., 2009). Up-scaling a site-specific model is often limited partly by lack of localized spatial dataset with high accuracy ε_{max} that fully considers spatial heterogeneity of landscape. The spatial dataset of ε_{max} we generated in this study provides a new opportunity for up-scaling of site-specific model to regional scale with integrated multi-site EC measurements and satellite observation.

As the LUE-based remote sensing models become important methods for estimating regional GPP, the critical assumption made for LUE-based models should be a concern or reexamined (Ahl et al., 2004; Drolet et al., 2008). ε_{max} in LUE-based models needs to fully consider the spatial heterogeneity of vegetation, plant function groups, and their texture (fractional cover) (Trotter et al., 2002). In current LUE-based models, ε_{max} is determined by "ideal" land cover or biome types that do not vary with space or time. However, in the real world ε_{max} is rather a variable than a constant even in the same vegetation type in the same biome. It varies with canopy densities, ages, and nutrient level from pixel to pixel and from time to time. Moreover, the accuracy of land cover types that ε_{max} relies on in LUE-based models should also be a concern. The simulated GPP of a mixed pixel suffers from uncertainties caused by mixed ε_{max}. This is also a major problem that most LUE-based GPP models face.

In this study, we used a dynamic modeling method that employs minimal visible albedo and maximal EVI in growing season to get ε_{max} for each pixel. Considering the visible albedo and EVI having the ability of representing mixed information for every pixel, the mixed signals of ε_{max} could also be captured even over complex landscape by our method. We hope this dynamic modeling method could to some extent improve regional GPP modeling by introducing pixel level ε_{max} with full consideration of its heterogeneous nature.

Acknowledgments

This study was supported by the National Basic Research Program of China (Nos. 2009CB723904 and 2006CB400500). The field measurements of GPP were provided by 14 participant flux sites under the Enhanced Coordinated Observation of Land–Atmospheric Interactions project.

References

Aber, J. D., Reich, P. B., & Goulden, M. L. (1996). Extrapolating leaf CO_2 exchange to the canopy: A generalized model of forest photosynthesis compared with measurements by eddy correlation. *Oecologia*, *106*, 257−265.

Ahl, D. E., Gower, S. T., Mackay, D. S., Burrows, S. N., Norman, J. M., & Diak, G. R. (2004). Heterogeneity of light use efficiency in a northern Wisconsin forest: implications for modeling net primary production with remote sensing. *Remote Sensing of Environment*, *93*, 168−178.

Chasmer, L., Barr, A., Hopkinson, C., McCaughey, H., Treitz, P., Black, A., et al. (2009). Scaling and assessment of GPP from MODIS using a combination of airborne lidar and eddy covariance measurements over jack pine forests. *Remote Sensing of Environment*, *113*, 82−93.

Cheng, Y. B., Middleton, E. M., Hilker, T., Coops, N. C., Black, T. A., & Krishnan, P. (2009). Dynamics of spectral bio-indicators and their correlations with light use efficiency using directional observations at a Douglas-fir forest. *Measurement Science and Technology*, *20*(095107), 15.

Coops, N. C., Ferster, C. J., Waring, R. H., & Nightingale, J. (2009). Comparison of three models for predicting gross primary production across and within forested ecoregions in the contiguous United States. *Remote Sensing of Environment*, *113*, 680−690.

Drolet, G. G., Huemmrich, K. F., Hall, F. G., Middleton, E. M., Black, T. A., Barr, A. G., et al. (2005). A MODIS-derived photochemical reflectance index to detect inter-annual variations in the photosynthetic light-use efficiency of a boreal deciduous forest. *Remote Sensing of Environment*, *98*, 212−224.

Drolet, G. G., Middleton, E. M., Huemmrich, K. F., Hall, F. G., Amiro, B. D., Barr, A. G., et al. (2008). Regional mapping of gross light-use efficiency using MODIS spectral indices. *Remote Sensing of Environment*, *112*, 3064−3078.

Falge, E., Baldocchi, D., Olson, R., Anthoni, P., Aubinet, M., Bernhofer, C., et al. (2001). Gap filling strategies for defensible annual sums of net ecosystem exchange. *Agricultural and Forest Meteorology*, *107*, 43−69.

Falge, E., Baldocchi, D., Tenhunen, J., Aubinet, M., Bakwin, P., Berbigier, P., et al. (2002). Seasonality of ecosystem respiration and gross primary production as derived from FLUXNET measurements. *Agricultural and Forest Meteorology*, *113*, 53−74.

Falge, E., Tenhunen, J., Baldocchi, D., Aubinet, M., Bakwin, P., Berbigier, P., et al. (2002). Phase and amplitude of ecosystem carbon release and uptake potentials as derived from FLUXNET measurements. *Agricultural and Forest Meteorology*, *113*, 75−95.

Garbulsky, M. F., Penuelas, J., Papale, D., & Filella, I. (2008). Remote estimation of carbon dioxide uptake by a Mediterranean forest. *Global Change Biology*, *14*, 2860−2867.

Heinsch, F. A., Zhao, M. S., Running, S. W., Kimball, J. S., Nemani, R. R., Davis, K. J., et al. (2006). Evaluation of remote sensing based terrestrial productivity from MODIS using regional tower eddy flux network observations. *IEEE Transactions on Geoscience and Remote Sensing*, *44*, 1908−1925.

Huete, A., Didan, K., Miura, T., Rodriguez, E. P., Gao, X., & Ferreira, L. G. (2002). Overview of the radiometric and biophysical performance of the MODIS vegetation indices. *Remote Sensing of Environment*, *83*, 195−213.

Jenkins, J. P., Richardson, A. D., Braswell, B. H., Ollinger, S. V., Hollinger, D. Y., & Smith, M. L. (2007). Refining light-use efficiency calculations over a deciduous forest canopy using simultaneous tower-based carbon flux and radiometric measurements. *Agricultural and Forest Meteorology*, *143*, 64−79.

Jung, M., Verstraete, M., Gobron, N., Reichstein, M., Papale, D., Bondeau, A., et al. (2008). Diagnostic assessment of European gross primary production. *Global Change Biology*, *14*, 2349−2364.

Landsberg, J. J., & Waring, R. H. (1997). A generalised model of forest productivity using simplified concepts of radiation-use efficiency, carbon balance and partitioning. *Forest Ecology and Management*, *95*, 209−228.

Li, Z. Q., Yu, G. R., Xiao, X. M., Li, Y. N., Zhao, X. Q., Ren, C. Y., et al. (2007). Modeling gross primary production of alpine ecosystems in the Tibetan Plateau using MODIS images and climate data. *Remote Sensing of Environment*, *107*, 510−519.

Liang, S. L. (2000). Narrowband to broadband conversions of land surface albedo I algorithms. *Remote Sensing of Environment*, *76*, 213−238.

Liu, H. Z., Tu, G., Fu, C. B., & Shi, L. Q. (2008). Three-year variations of water, energy and fuxes of cropland and degraded grassland surfaces in a semi-arid area of northeastern China. *Advances in Atmospheric Sciences*, *25*(6), 1009−1020.

Maki, M., Ishiahra, M., & Tamura, M. (2004). Estimation of leaf water status to monitor the risk of forest fires by using remotely sensed data. *Remote Sensing of Environment*, *90*, 441−450.

Maselli, F., Papale, D., Puletti, N., Chirici, G., & Corona, P. (2009). Combining remote sensing and ancillary data to monitor the gross productivity of water-limited forest ecosystems. *Remote Sensing of Environment*, *113*, 657−667.

Nakaji, T., Ide, R., Oguma, H., Saigusa, N., & Fujinuma, Y. (2007). Utility of spectral vegetation index for estimation of gross CO_2 flux under varied sky conditions. *Remote Sensing of Environment*, *109*, 274−284.

Okin, G. S. (2007). Relative spectral mixture analysis—A multitemporal index of total vegetation cover. *Remote Sensing of Environment*, *106*, 467−479.

Potter, C. S., Randerson, J. T., Field, C. B., Matson, P. A., Vitousek, P. M., Mooney, et al. (1993). Terrestrial ecosystem production: A process model based on global satellite and surface data. *Global Biogeochemical Cycles*, *7*(4), 811−841.

Prince, S. D., & Goward, S. N. (1995). Global primary production: A remote sensing approach. *Journal of Biogeography*, *22*, 815−835.

Running, S. W., Nemani, R., Glassy, J. M., & Thornton, P. E. (1999). MODIS daily photosynthesis (PSN) and annual net primary production (NPP) product (MOD17), algorithm theoretical basis document, version 3.0. http://modis.gsfc.nasa.gov/

Running, S. W., Nemani, R. R., Heinsch, F. A., Zhao, M. S., Reeves, M., & Hashimoto, H. (2004). A continuous satellite-derived measure of global terrestrial primary production. *Bioscience*, *54*, 547−560.

Sellers, P., Dickinson, R., & Randall, D. (1997). Modeling the exchanges of energy, water and carbon between continents and the atmosphere. *Science*, *275*, 502−509.

Sims, D. A., Rahman, A. F., Cordova, V. D., El-Masri, B. Z., Baldocchi, D. D., Flanagan, L. B., et al. (2006). On the use of MODIS EVI to assess gross primary productivity of North American ecosystems. *Journal of Geophysical Research*, *111*, G04015, doi:10.1029/2006JG000162.

Sims, D. A., Rahman, A. F., Cordova, V. D., El-Masri, B. Z., Baldocchi, D. D., Bolstad, P. V., et al. (2008). A new model of gross primary productivity for North American ecosystems based solely on the enhanced vegetation index and land surface temperature from MODIS. *Remote Sensing of Environment*, *112*, 1633−1646.

Tian, Y., Dickinson, R. E., Zhou, L., Zeng, X., Dai, Y., Myneni, R. B., et al. (2004). Comparison of seasonal and spatial variations of leaf area index and fraction of absorbed photosynthetically active radiation from Moderate Resolution Imaging Spectroradiometer (MODIS) and Common Land Model. *Journal of Geophysical Research*, *109*, D01103, doi:10.1029/2003JD003777.

Trotter, G. M., Whitehead, D., & Pinkney, E. J. (2002). The photochemical reflectance index as a measure of photosynthetic light use efficiency for plants with varying foliar nitrogen contents. *International Journal of Remote Sensing*, *23*, 1207−1212.

Turner, D. P., Ritts, W. D., Cohen, W. B., Gower, S. T., Zhao, M. S., Running, S. W., et al. (2003). Scaling gross primary production (GPP) over boreal and deciduous forest landscapes in support of MODIS GPP product validation. *Remote Sensing of Environment*, *88*, 256−270.

Turner, D. P., Ritts, W. D., Cohen, W. B., Maeirsperger, T. K., Gower, S. T., Kirschbaum, A. A., et al. (2005). Site-level evaluation of satellite-based global terrestrial gross primary production and net primary production monitoring. *Global Change Biology*, *11*, 666−684.

Veroustraete, F., Sabbe, H., & Eerens, H. (2002). Estimation of carbon mass fluxes over Europe using the C-Fix model and Euroflux data. *Remote Sensing of Environment*, *83*, 376−399.

Webb, E. K., Pearman, G. I., & Leuning, R. (1980). Correction of flux measurements for density effects due to heat and water vapour transfer. *Quarterly Journal of the Royal Meteorological Society*, *106*, 85−100.

Wu, J. B., Xiao, X. M., Guan, D. X., Shi, T. T., Jin, C. J., & Han, S. J. (2009). Estimation of the gross primary production of an old-growth temperate mixed forest using eddy covariance and remote sensing. *International Journal of Remote Sensing*, *30*, 463−479.

Xiao, X. M., Hollinger, D., Aber, J., Goltz, M., Davidson, E. A., Zhang, Q. Y., et al. (2004). Satellite-based modeling of gross primary production in an evergreen needleleaf forest. *Remote Sensing of Environment*, *89*, 519−534.

Xiao, X. M., Zhang, Q. Y., Braswell, B., Urbanski, S., Boles, S., Wofsy, S., et al. (2004). Modeling gross primary production of temperate deciduous broadleaf forest using satellite images and climate data. *Remote Sensing of Environment*, *91*, 256−270.

Yan, H. M., Fu, Y. L., Xiao, X. M., Huang, H. Q., He, H. L., & Ediger, L. (2009). Modeling gross primary productivity for winter wheat–maize double cropping System using MODIS time series and CO_2 eddy flux tower data. *Agriculture Ecosystems and Environment*, *129*, 391−400.

Zhang, X. Y., Friedl, M. A., Schaaf, C. B., Strahler, A. H., Hodges, J. C. F., Gao, F., et al. (2003). Monitoring vegetation phenology using MODIS. *Remote Sensing of Environment*, *84*, 471−475.